This article has been accepted for publication in a future issue of this journal, but has not been fully edited. Content may change prior to final publication. Citation information: DOI 10.1109/JERM.2019.2896719, IEEE Journal of Electromagnetics, RF and Microwaves in Medicine and Biology

Measurement of Ion-Pairing Interactions in Buffer Solutions with Microwave Microfluidics

Charles A. E. Little, Angela C. Stelson, Nathan D. Orloff, Christian J. Long, James C. Booth

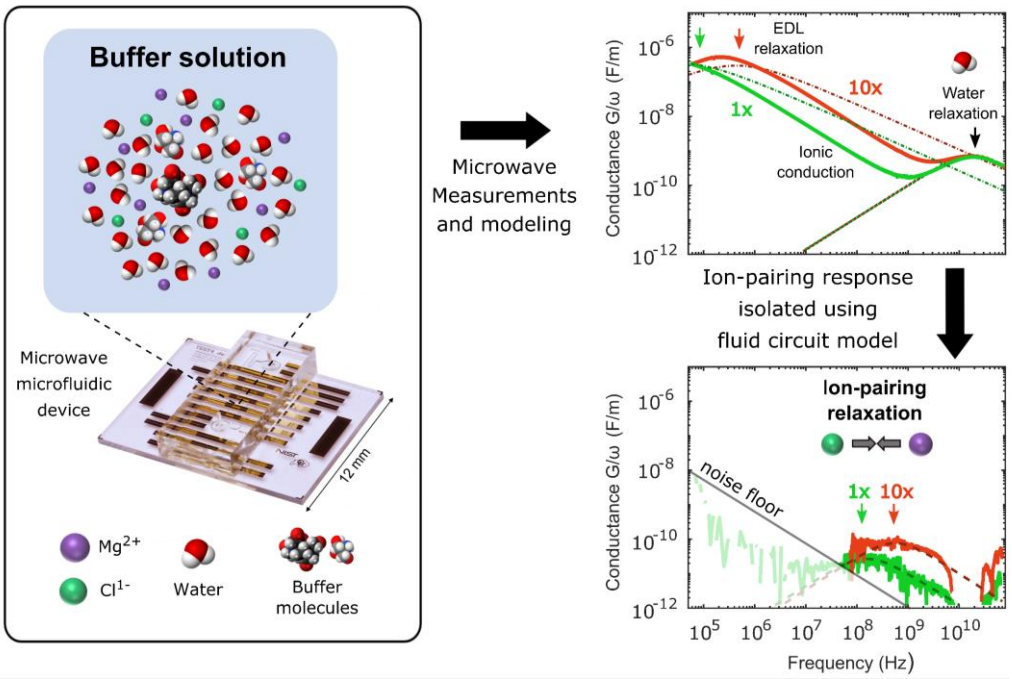

Modeling broadband admittance to isolate weak ion-pairing response.

Take-Home Messages

- Our microwave microfluidics device paired with on-chip calibrations enable admittance measurements of fluids over a six-decade frequency range (40 kHz to 67 GHz).
- We use our microwave microfluidics devices to characterize weak ion-pairing interactions in nanoliter volumes of common buffer solutions *in situ* and non-destructively.
- Buffer solutions are ubiquitous in biological systems and quantifying their electrical and ionic properties enables future studies of ion dynamics in biomolecular systems.
- These broadband measurements can inform more narrowband measurements of biological, biochemical, and pharmaceutical fluid systems, which may be more cost-effective and lead to real-time assessment of biological systems.

2469-7249 (c) 2018 IEEE. Personal use is permitted, but republication/redistribution requires IEEE permission. See http://www.ieee.org/publications_standards/publications/rights/index.html for more information.

This article has been accepted for publication in a future issue of this journal, but has not been fully edited. Content may change prior to final publication. Citation information: DOI 10.1109/JERM.2019.2896719, IEEE Journal of Electromagnetics, RF and Microwaves in Medicine and Biology

Measurement of Ion-Pairing Interactions in Buffer Solutions with Microwave Microfluidics

Charles A. E. Little [1], Angela C. Stelson [1], Nathan D. Orloff [1], Christian J. Long [1], James C. Booth [1*]

Abstract Microwave microfluidic spectroscopy is an emerging technique for quantifying the frequency-dependent electrical response of fluids. This technique can access important physical properties including ion mobility and hydration, which are directly applicable to biochemistry. One critical step towards quantifying these effects is to develop accurate models for the behavior of buffer solutions containing mobile ions. Here, we show that ions in buffer solutions produce a weak ion-pairing response. We used microfluidic channels integrated with coplanar waveguides in combination with a hybrid microwave calibration protocol to extract the broadband microwave admittance spectra of a standard TAE-Mg^{2+} buffer solution between 100 kHz and 67 GHz. To characterize the ion-pairing response, we fit the calibrated admittance data with two models: a conventional model without ion-pairing and with a water relaxation described by a 'Cole-Cole' function, to our alternative model that includes ion-pairing and a single Debye-type water relaxation. Including ion-pairing improved the goodness of fit across the entire frequency range. In the higher concentration buffer solution, we saw a reduction in the max systematic error in the fit residuals from 10 % to less than 4 %. The measurement and fitting techniques are widely applicable, providing critical information about the behavior of solvated ions.

Keywords **— Microfluidics, Impedance measurement, Permittivity, Chemical and biological sensors, Microwave measurements**

I. Introduction

MICROWAVE microfluidic spectroscopy [1]–[5] is a promising means of detecting and characterizing weak, non-covalent interactions in solution. For example, pairs of ions in solution can form a transient non-covalent bond. This phenomenon is commonly referred to as ion-pairing (IP) [6]–[8]. Quantifying IP is critical to understanding the dynamics of ions in solution. Interferometer-based microwave dielectric spectroscopy has been used to observe IP in a variety of salt solutions [6]–[8]; however, this technique operates over a limited frequency range, spanning only three orders of magnitude (typically from 200 MHz to 100 GHz) [6], [9]. Recent advances in on-chip microwave metrology have enabled broadband measurements over a continuous frequency range from DC to 67 GHz [3], [4], [10]. A greater frequency range allows us to better distinguish various charged-based mechanisms, whose effects may overlap at any given frequency.

We use multiple coplanar waveguide (CPW) structures integrated with microfluidic channels to measure the broadband electrical properties of aqueous solutions containing tris-acetate-ethylenediaminetetraacetic acid with magnesium (TAE-Mg^{2+}), a common buffer for DNA and RNA solutions [11]. Our frequency span (100 kHz to 67 GHz) covers three main ranges: a low-frequency range where electrical double-layer (EDL) effects between the solution and electrodes occur, an intermediate frequency range where we primarily see the bulk ionic conductivity of the fluid, and a high-frequency range dominated by the relaxation of water. We expected the effects of IP to overlap with ionic conductivity and water relaxation effects in a frequency range between 100 MHz and 10 GHz [9].

Here, we quantified charge-based effects present in the electrical response of our buffer solutions by fitting the measured frequency-dependent admittance with a model that includes an EDL relaxation, ionic conductivity effects, and water relaxation [3]. We included an additional relaxation to account for the presence of IP [9] and compared the goodness of fit for a model with and without IP to validate our detection of a weak IP response. Including the IP relaxation improved the goodness of fit in the IP regime, as well as over the entire measurement frequency range. These results illustrate the necessity of including IP in future models of ionic solutions.

This paper is expanded from the 2018 International Microwave Biomedical Conference (IMBioC) [12]. Here, we report on results of measurements of an additional concentration of buffer solution (10× the concentration of the standard buffer solution). The 10× solution is used to emphasize the necessity of including IP in broadband models of ionic solutions. In addition, we include tables of fit parameters and uncertainties to quantify the change in the broadband admittance with concentration.

1Communication Technology Laboratory, National Institute of Standards and Technology, Boulder, CO 80305 USA.

*Corresponding author: Dr. James C. Booth, National Institute of Standards and Technology, 325 Broadway, Stop 672.01, Boulder, CO 80305. (e-mail: james.booth@nist.gov).

All authors are with the National Institute of Standards and Technology, 325 Broadway, Stop 672.01, Boulder, CO 80305 (e-mail addresses in order: {cully.little},{angela.stelson},{nathan.orloff},{Christian.long}@nist.gov).

This paper is an expanded paper from the IEEE IMBioC 2018, Philadelphia, PA.

This paper is an official contribution of NIST; not subject to copyright in the US. Usage of commercial products herein is for information only; it does not imply recommendation or endorsement by NIST.

2469-7249 (c) 2018 IEEE. Personal use is permitted, but republication/redistribution requires IEEE permission. See http://www.ieee.org/publications_standards/publications/rights/index.html for more information.

This article has been accepted for publication in a future issue of this journal, but has not been fully edited. Content may change prior to final publication. Citation information: DOI 10.1109/JERM.2019.2896719, IEEE Journal of Electromagnetics, RF and Microwaves in Medicine and Biology

II. Methods

A. Device Fabrication

The microwave-microfluidics devices used here were detailed extensively in previous work [3]. Briefly, all CPW structures on our devices were fabricated on the same fused-silica substrate, with 50 µm wide center conductors, 200 µm wide ground planes, and 5 µm wide gaps between the center conductors and ground planes. Bare CPW lines (*i.e.*, a continuous CPW without microfluidics) had a characteristic impedance of approximately 50 Ω. The microwave calibrations we performed required multiple CPW structures including CPW lines of different lengths, a series-resistor, a series-capacitor, and a short-circuit-reflect. Optimal CPW line lengths were selected to minimize calibration uncertainty.

We fabricated all bare CPW structures on a 12-mm square chip (referred to as the "reference chip"). The microfluidics-loaded CPW structures were fabricated on a separate 12-mm square chip (referred to as the "test chip"). The reference and test chips were co-fabricated on the same fused-silica wafer to ensure uniformity between CPW structures. The microfluidic channels on the test chip were fabricated in two layers: a bottom layer consisting of 50 µm tall channels made from SU-8 (a photo-definable epoxy-based polymer), and a top layer with 50 µm tall channels patterned in poly(dimethylsiloxane) (PDMS) (Fig. 1B). The SU-8 microfluidic channels were ~80 µm wide, with lengths of 0.540 mm, 0.664 mm, 1.324 mm, 1.984 mm, and 3.134 mm (±0.005 mm). Various channel lengths were required for a multiline-TRL calibration [13] on the microfluidics-loaded CPW devices, discussed further in the next section. The CPW gap width and SU-8 channel height ensured that the electromagnetic fields interact primarily with fluids within the lower SU-8 channels, rather than the upper PDMS layer.

B. Microwave Measurements and Calibrations

We made electrical connection to each CPW structure with movable microwave probes mounted on a temperature-controlled probe stage set to 25 °C (Fig. 1A). A vector network analyzer (VNA) in a 2-port configuration was used to measure raw scattering parameters (S-parameters) for each CPW structure over 640 frequency points from 40 kHz to 67 GHz on a logarithmic frequency scale. The incident RF power was -15 dBm, and data was collected with a resolution bandwidth of 10 Hz. The absolute temperature within the channels was known to within ± 2 °C (determined in previous work [3]).

At high frequencies (> 1 GHz), we performed a multiline-TRL calibration on the reference chip to determine the frequency-dependent propagation constant for the bare CPW lines (γ_0) [13], [14]. We also performed a multiline-TRL calibration on the test chip to determine the propagation constant for the microfluidic-loaded CPW lines (γ_{tot}). Additionally, a series-resistor calibration was performed on the reference chip to determine the frequency-dependent capacitance per unit length (C_0) for the bare CPW lines [15].

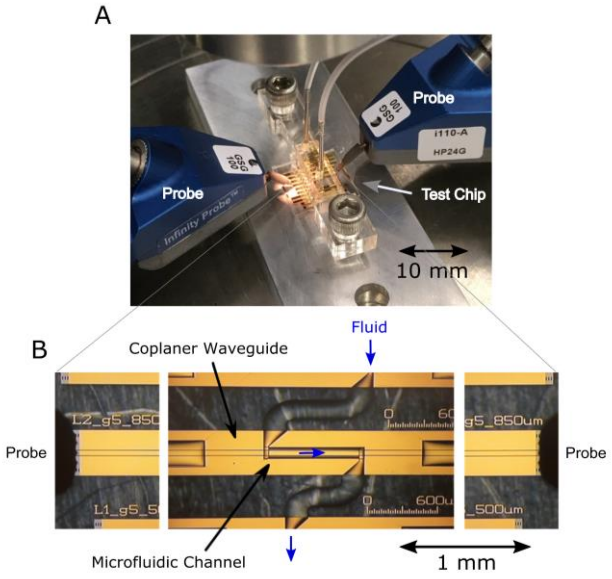

Fig. 1. Images of the device used in this work A) photograph of the assembled microfluidics device during measurement. B) Stitched microscope image of a single CPW line with microfluidic channels. The image shows microwave probe landings as well as the direction of fluid flow over the CPW structure.

Empirically, we find that C_0 has a constant value over the measurement range.

We assumed a negligible conductance per unit length (G_0) for the bare CPW lines (reference chip) due to the low dielectric loss of the fused-silica substrate. Therefore, the propagation constant γ_0 for the bare CPW line can be written as:

$$\gamma_0 = \sqrt{(R_0 + i\omega L_0) i\omega C_0}, \qquad (1)$$

where ω is the angular frequency and R_0 and L_0 are the frequency-dependent distributed resistance and inductance per unit length of the bare CPW devices, respectively. As the channel and fluid have negligible magnetic response, we could assume that R_0 and L_0 are the same for the reference and test chips. Under this assumption:

$$\gamma_{tot} = \sqrt{(R_0 + i\omega L_0)(G_{tot} + i\omega C_{tot})}, \quad (2)$$

where G_{tot} and C_{tot} are the frequency-dependent distributed conductance and capacitance per unit length of the fluid-loaded CPW devices, respectively. We combined Eqs. (1) and (2), to solve for G_{tot} and C_{tot} in terms of the measured quantities γ_0, γ_{tot}, and C_0. The total frequency-dependent admittance Y_{tot} of the device can then be given as:

$$Y_{tot} = G_{tot} + i\omega C_{tot} = \frac{\gamma_{tot}^2}{\gamma_0^2} \cdot i\omega C_o. \qquad (3)$$

The methods and procedures employed here for both the multiline-TRL and series-resistor calibrations are identical to those outlined by DeGroot et al. [14] and Orloff et al. [15] respectively. In short, the series-resistor calibration assumes

2469-7249 (c) 2018 IEEE. Personal use is permitted, but republication/redistribution requires IEEE permission. See http://www.ieee.org/publications_standards/publications/rights/index.html for more information.

This article has been accepted for publication in a future issue of this journal, but has not been fully edited. Content may change prior to final publication. Citation information: DOI 10.1109/JERM.2019.2896719, IEEE Journal of Electromagnetics, RF and Microwaves in Medicine and Biology

that the impedance of the series-resistor is approximately equal to the DC resistance (R_{DC}) of the series-resistor element (~50 Ω). The exact value of R_{DC} was measured directly, as R_{DC} can vary between devices. At high frequencies, the series-resistor algorithm used γ_0 (calculated directly from multiline-TRL), in addition to measured R_{DC}, to calculate a value for C_0.

For low frequencies (<1 GHz), we used a separate calibration process known as de-embedding, wherein the raw S-parameter measurements for each CPW line were error-corrected by accounting for the effects of cables, probes, and CPW sections leading up to the line. Mathematically, we used a transmission matrix (T-matrix) formalism to build a series of cascade matrices that represent the total response of the line. The individual T-matrices in the cascade each capture the responses of the various sections: the transmission line up to the probe tips, the bare CPW sections, and the SU-8 covered CPW sections. The error correction up to the probe tips (error boxes) were first determined from measurements of the series-resistor and series-capacitor structures as part of the series-resistor calibration [15]. To determine the distributed circuit parameters G_{tot} and C_{tot} from the de-embedded S-parameters, we performed a nonlinear least-squares optimization, comparing the response of an ideal transmission line to our de-embedded S-parameters, holding $R_{tot} = R_0$ and $L_{tot} = L_0$. A more detailed explanation of the least-squares method is given by Liu et al. [4] and Orloff et al [16]. We separately used the de-embedding process, in combination with the least-squares method, on a single line covered with SU-8 and a single bare CPW line to determine the impedance and propagation constant of the SU-8 covered sections and bare CPW sections, respectively. The extracted propagation constants were then used to account for the bare CPW section and short SU-8 covered section leading from the probe tips up to the microfluidic channels.

C. Equivalent-Circuit Model

An equivalent-circuit model (Fig. 2) was used to describe the frequency-dependent electrical response of our microfluidics-loaded CPW lines (Y_{tot}). By fitting this model to our calibrated broadband admittance data, we can extract equivalent circuit parameters that relate to the physical properties of the fluid.

The total admittance of the fluid-loaded devices (Y_{tot}) is (Fig. 2A):

$$Y_{tot} = \left(\frac{2}{Y_{EDL}} + \frac{1}{Y_f}\right)^{-1}, \quad (4)$$

where Y_{EDL} is the admittance of the EDL at the interface between electrodes and fluid and Y_f is the admittance of the bulk fluid. Here, we model the fluid admittance (Y_f) as (Fig. 2B):

$$Y_f = Y_{IP} + Y_w + G_\sigma + \mathrm{i}\omega C_\infty, \quad (5)$$

where Y_{IP} is the IP relaxation admittance, Y_w is the water relaxation admittance, G_σ is the ionic conductivity per unit length, and C_∞ is the frequency-independent capacitance per unit length at frequencies above the measurement range. In our previous work we focused on validating our model for the EDL [3], and did not include a term for Y_{IP}.

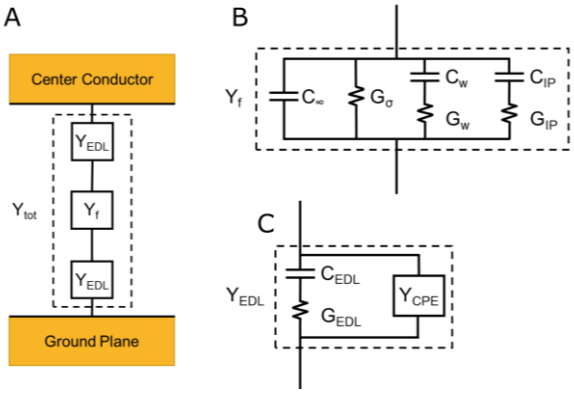

Fig. 2. Equivalent circuit model describing the admittance of the microfluidic channels. A) The bulk admittance of the fluid (Y_f) is in series with the admittances of the electrical double-layers (Y_{EDL}), which form on the center conductor and ground planes. B) The equivalent circuit model for Y_f. C) The equivalent circuit model for Y_{EDL}.

In general, relaxation phenomena can be described by the Cole-Cole or Debye models, where the Cole-Cole model is an expansion of the Debye model to allow for a distribution of relaxation times. Previous studies have fit IP with a Debye relaxation [9], [17], while the admittance of water is commonly fit with a Cole-Cole expression [18]. We expanded Eq. 5 to explicitly state the frequency-independent fit parameters in the model:

$$Y_f(\omega) = \mathrm{i}\omega\frac{\Delta C_{IP}}{1+(\mathrm{i}\omega\tau_{IP})} + \mathrm{i}\omega\frac{\Delta C_w}{1+(\mathrm{i}\omega\tau_w)^{(1-\alpha_w)}} + G_\sigma + i\omega C_\infty, \quad (6)$$

where ΔC_w is the magnitude of the water relaxation, and ΔC_{IP} is the magnitude of the IP relaxation. The fit parameters ΔC_w and ΔC_{IP} are frequency independent and should not be confused with the frequency dependent equivalent circuit elements C_w and C_{IP}. The time constants in Eq. 6 (τ_w and τ_{IP}) are the relaxation times for water and IP respectively. The Cole-Cole expression for the water relaxation includes a shape-broadening parameter α_w, where $\alpha_w = 0$ is equivalent to a pure Debye relaxation and $\alpha_w > 0$ corresponds to a Cole-Cole relaxation with a distribution of relaxation times. The depiction in Fig. 2B assumes $\alpha_w = 0$, *i.e.*, a pure Debye relaxation. An accurate representation of the Cole-Cole relaxation in equivalent circuit form would require an infinite series of parallel C_w and G_w circuit elements. We emphasize that we fit both the real and imaginary parts of the measured frequency-dependent admittance per unit length to the real and imaginary parts of the frequency-dependent Debye or Cole-Cole functions.

The EDL admittance can also be modelled with a Cole-Cole expression [3]:

$$Y_{EDL}(\omega) = \mathrm{i}\omega\frac{\Delta C_{EDL}}{1+(\mathrm{i}\omega\tau_{EDL})^{(1-\alpha_{EDL})}} + Y_{CPE}, \quad (7)$$

2469-7249 (c) 2018 IEEE. Personal use is permitted, but republication/redistribution requires IEEE permission. See http://www.ieee.org/publications_standards/publications/rights/index.html for more information.

This article has been accepted for publication in a future issue of this journal, but has not been fully edited. Content may change prior to final publication. Citation information: DOI 10.1109/JERM.2019.2896719, IEEE Journal of Electromagnetics, RF and Microwaves in Medicine and Biology

where ΔC_{EDL} is the magnitude of the EDL relaxation, α_{EDL} is the EDL shape-broadening parameter, and τ_{EDL} is the relaxation time associated with the EDL. As with ΔC_w and ΔC_{IP}, ΔC_{EDL} should not be confused with C_{EDL}. In parallel with the EDL relaxation (Fig. 2C and Eq. 7), we included a constant phase element Y_{CPE} (Fig. 2C) [19][3]:

$$Y_{CPE}(\omega) = Q_{CPE}\omega^n e^{i\frac{\pi}{2}n}, \quad (8)$$

where Q_{CPE} is the magnitude of the CPE admittance, and n describes the phase of the CPE. Eq. 8 is a common phenomenological expression for CPW admittance which adequately describes the EDL response [3]. When we allowed n to vary as a fit parameter, values for n ranged between 0.98 and 1. To reduce the number of fit parameters, we assumed a fully-capacitive CPE admittance, *i.e.*, $n = 1$.

D. Sample Preparation

We measured two concentrations of aqueous TAE-Mg^{2+} buffer solutions [20]. The first solution (1×) consisted of: 40 mol/m^3 Tris (tris(hydroxymethyl)aminomethane), 2 mol/m^3 EDTA (Ethylenediaminetetraacetic acid), 2 mol/m^3 NaCl, and 12.5 mol/m^3 $MgCl_2$. The 1× concentration is standard in the preparation of DNA and RNA [11]. All solute concentrations were increased ten-fold for the second solution (10×). We expected the 10× solution to have a larger ΔC_{IP} than the 1× solution. We also expected a shorter IP relaxation time (τ_{IP}) for the 10× vs. 1× solutions, *i.e.*, the IP relaxation would appear at higher frequencies.

III. Results

A. Competing Models for Fluid Admittance:

To test the hypothesis that IP should be included in our model for Y_{tot}, we compared two models. In the first model (referred to here as 'Cole-Cole') we assumed that there was no IP ($Y_{IP} = 0$) and allowed α_w to vary. In the second model (referred to here as 'Debye+IP') we included an expression for Y_{IP} and set $\alpha_w = 0$. By setting $\alpha_w = 0$, we assumed that both IP and water relaxations are pure Debye-type relaxation phenomena, and that the distribution in the Cole-Cole expression may compensate for the presence of IP interactions in the admittance data.

B. Fitting Y_{tot} with the Debye + IP model

The calibrated data for the TAE-Mg^{2+} 1× concentration is shown in Fig. 3A, where C_{tot} and G_{tot}/ω are linearly proportional to the real and imaginary parts of the fluid permittivity, ϵ' and ϵ'', respectively [3]. Qualitatively, we interpret the data as having three frequency regimes. At low frequencies (below 10 MHz), EDL effects are noticeable. At intermediate frequencies (between 10 MHz and 1 GHz), we see effects from the conductivity of ions in the bulk fluid. At high frequencies (~20 GHz), the primary feature is the relaxation of water molecules. The relaxation associated with IP was predicted to be between 200 MHz to 700 MHz [9], and was not immediately apparent in the calibrated data in Fig. 3A.

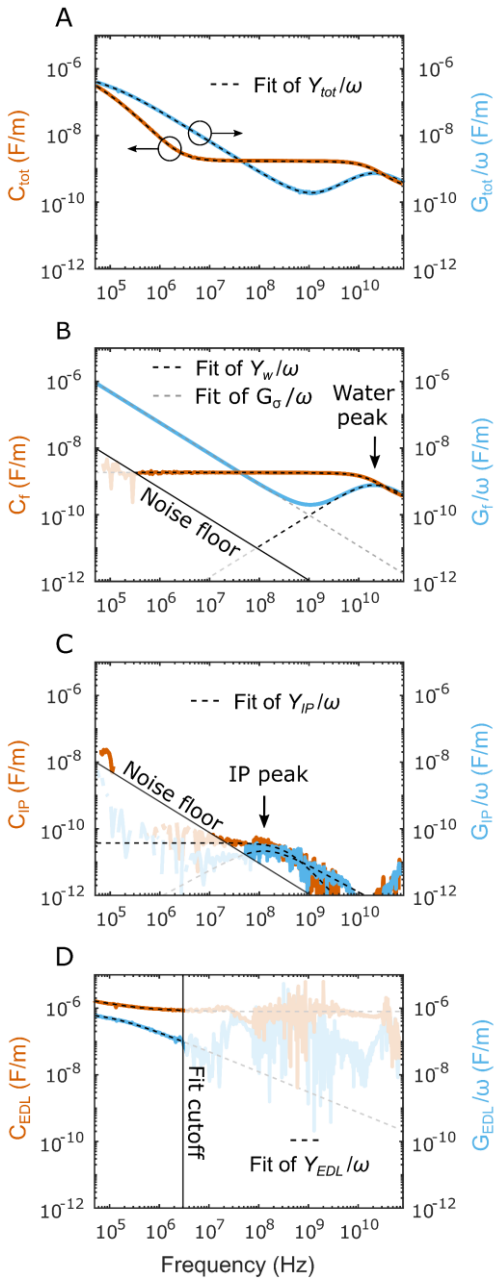

Fig. 3. Admittance data and fittings for the 1× concentration: Y_{tot} (A), Y_f (B), Y_{IP} (C), and Y_{EDL} (D). The complex components of the admittance data are plotted in terms of capacitance per unit length (C_{tot}), and conductance per unit length divided by angular frequency (G_{tot}/ω). A) measured Y_{tot} data, with fit of Y_{tot}. B) extracted data for Y_f overlaid with fits for the water admittance (Y_w) and ionic conductance (G_σ/ω). C) extracted data for Y_{IP} with fit of Y_{IP}. D) extracted Y_{EDL} data with fit of Y_{EDL}. Extracted data in plots B, C, and D were constructed by eliminating the other components of Y_{tot} using fit curves. White shaded areas indicate regions of low signal-to-noise.

The total fits of the real and imaginary parts of the admittance C_{tot} and G_{tot}/ω for the 'Debye + IP' model (Fig. 3B) are in good agreement with the calibrated admittance data over the entire frequency range. To model Y_{tot}, we had to fit both parts of the complex admittance simultaneously across the entire frequency range. To visualize the

2469-7249 (c) 2018 IEEE. Personal use is permitted, but republication/redistribution requires IEEE permission. See http://www.ieee.org/publications_standards/publications/rights/index.html for more information.

This article has been accepted for publication in a future issue of this journal, but has not been fully edited. Content may change prior to final publication. Citation information: DOI 10.1109/JERM.2019.2896719, IEEE Journal of Electromagnetics, RF and Microwaves in Medicine and Biology

contribution of each component to the total admittance (Eq. 4), we plot each component of the fit in Fig. 3. By removing the fit of Y_{EDL} from measured Y_{tot} data, we can isolate data associated with Y_{f} (Figs. 3B), from which we found good agreement with the model across the entire frequency range. In Fig. 3D, we removed the fit of Y_{f} from measured Y_{tot} data to isolate the effects of the EDL.

Finally, we show the isolated data associated with IP in Fig. 3C, in which we see a clear relaxation peak in both C_{IP} and G_{IP}/ω above the noise floor of the measurement (white shaded region in Fig. 3C). We found good agreement between isolated data and the fit of C_{tot} and G_{tot}/ω. The fit calculated an IP relaxation peak at 265 ± 20 MHz for the 1× concentration and 637 ± 88 MHz for the 10× concentration. Because this buffer solution is a complex mixture of charged species, the specific mechanism of IP for this sample was difficult to identify. Fitting the data with multiple IP relaxations did not improve the overall fit, which suggests a single dominate IP mechanism.

TABLE I
FIT PARAMETERS FOR 1× CONCENTRATION

Fit Parameter	Value		Fit Error	Measurement Error
ΔC_w (F/m) × 10^{-10}	14.70	±	0.02	0.04
τ_w (s/rad) × 10^{-12}	9.59	±	0.01	0.01
C_∞ (F/m) × 10^{-10}	2.488	±	0.014	0.008
G_σ (S/m)	0.584	±	0.001	0.016
ΔC_{IP} (F/m) × 10^{-10}	0.52	±	0.02	0.09
τ_{IP} (s/rad) × 10^{-10}	6.0	±	0.5	0.9
ΔC_{EDL} (F/m) × 10^{-7}	24	±	1	1
τ_{EDL} (s/rad) × 10^{-6}	3.0	±	0.2	0.3
1 - α_{EDL}	0.666	±	0.014	0.009
Q_{CPE} (S m^{-1} Hz^{-1}) × 10^{-8}	71	±	1	3

Fit parameters for the 'Debye+IP' fit of admittance data. Fit error and measurement error correspond to a 95% confidence interval.

TABLE II
FIT PARAMETERS FOR 10× CONCENTRATION

Fit Parameter	Value		Fit Error	Measurement Error
ΔC_w (F/m) × 10^{-10}	13.39	±	0.04	0.09
τ_w (s/rad) × 10^{-12}	11.08	±	0.04	0.07
C_∞ (F/m) × 10^{-10}	2.519	±	0.032	0.007
G_σ (S/m)	3.64	±	0.01	0.08
ΔC_{IP} (F/m) × 10^{-10}	1.1	±	0.1	0.2
τ_{IP} (s/rad) × 10^{-10}	2.5	±	0.4	0.2
ΔC_{EDL} (F/m) × 10^{-7}	16.4	±	0.4	1.5
τ_{EDL} (s/rad) × 10^{-6}	0.20	±	0.01	0.02
1 - α_{EDL}	0.73	±	0.02	0.03
Q_{CPE} (S m^{-1} Hz^{-1}) × 10^{-8}	67	±	2	1

Fit parameters for the 'Debye+IP' fit of admittance data. Fit error and measurement error correspond to a 95% confidence interval.

The importance of the broadband measurement becomes evident when we compare Fig. 3B and 3C, where the data show the bulk fluid admittance and IP relaxation admittance respectively. In Fig. 3B, G_f/ω has a broad frequency dependence around the IP relaxation peak frequency (~265 MHz) and is significantly larger than the IP response (G_{IP}/ω) at these frequencies (Fig. 3C). Therefore, without spanning many orders of magnitude in frequency we would not be able to properly capture and separate each individual component of the admittance response. [12]

The resulting fit parameters for the 1× and 10× concentrations are provided in Table 1 and Table 2, respectively. Expanded errors (95% confidence interval) for each fit parameter value were determined from fit residuals (Fit Error in Tables 1 and 2), and from three repeat measurements at both concentrations (Measurement Error in Tables 1 and 2). Both the fit and measurement errors were small compared to extracted quantities, indicating that the model is consistent with the data and that all the parameters are well conditioned.

When we compared fit parameters between 1× and 10× concentrations, we found that all parameters significantly changed between concentrations, except for C_∞ and Q_{CPE}. When we increased concentration from 1× to 10× we saw that the ionic conductivity term G_σ also increases by a factor of 6.2; In a simple salt solution G_σ should be directly proportional to ionic concentration [21], while in a buffer solution this may not be the case due to the presence of multiple charge states of the buffer molecules. We saw that the magnitude of the water relaxation (ΔC_w) decreased by 9 %, and the peak of the relaxation decreased in frequency from (16.59 ± 0.02) GHz to (14.36 ± 0.05) GHz. Interpreting changes in the water relaxation is difficult as the exact dependence on ionic concentration is poorly understood and highly dependent on the type of salts used [3], [17]. The magnitude of the EDL relaxation (C_{EDL}) also decreased by 68 % and shifted in frequency from (53 ± 3) kHz to (796 ± 72) kHz, as expected from previous studies [3], [21]. We also saw an increase in 1-α_{EDL} from (67 ± 1) % to (73 ± 2) %, although the asymmetry in the EDL relaxation (1-α_{EDL}) is also poorly understood. Finally, we saw that the magnitude of the IP relaxation (ΔC_{IP}) increased by a factor of 2.1, and the peak of the relaxation shifted in frequency from (265 ± 20) MHz to (637 ± 88) MHz. Buchner et al. also reported an increase in frequency with concentration in the same frequency regime [6], although it is difficult to make a direct comparison.

C. Comparison of 'Debye + IP' and 'Cole-Cole' Models

To further validate the inclusion of an IP relaxation in our admittance model, we compared fit residuals as a function of frequency between the 'Cole-Cole' and 'Debye+IP' models for the 1× and 10× concentrations (Fig. 4). Residuals that are symmetric around zero are indicative of random error, *i.e.*, noise, while residuals that are asymmetrically distributed around zero are indicative of systematic error, perhaps resulting from a poor fit of the data. When we compare the

2469-7249 (c) 2018 IEEE. Personal use is permitted, but republication/redistribution requires IEEE permission. See http://www.ieee.org/publications_standards/publications/rights/index.html for more information.

This article has been accepted for publication in a future issue of this journal, but has not been fully edited. Content may change prior to final publication. Citation information: DOI 10.1109/JERM.2019.2896719, IEEE Journal of Electromagnetics, RF and Microwaves in Medicine and Biology

'Cole-Cole' model in Fig. 4A, to the 'Debye+IP' model in Fig. 4B, we can see that the residuals are more symmetric around zero for the 'Debye+IP' model, meaning we have reduced the overall systematic fitting error. We can also see in Fig. 4 that the 'Debye + IP' model produced a better fit over the entire frequency range, to a small degree in the 1× concentration (Fig. 4C and 4D), and to a large degree in the 10× concentration (Fig. 4E and 4F). In the 10× solution, the maximum residuals in the capacitance approached 10 % before the inclusion of an IP relaxation, and were reduced below 4 % after the inclusion of an IP relaxation. It is important to note that the 'Debye+IP' model included one extra degree of freedom compared with the 'Cole-Cole' model, which can reduce the overall residuals by overfitting. However, overfitting is unlikely as the IP peak is above the noise floor, and the IP peak is well fit in both C_{tot} and G_{tot}/ω by the additional relaxation (Figs. 3C), supporting the assertion that the extra Debye relaxation in the 'Debye+IP' model is a real feature of the admittance data. Again, the systematic errors were reduced throughout the frequency range, above and below the IP frequency regime for both concentrations, this shows the importance of including IP in our models of ionic solutions, not only to measure IP, but also to improve our fits of the EDL and water relaxation.

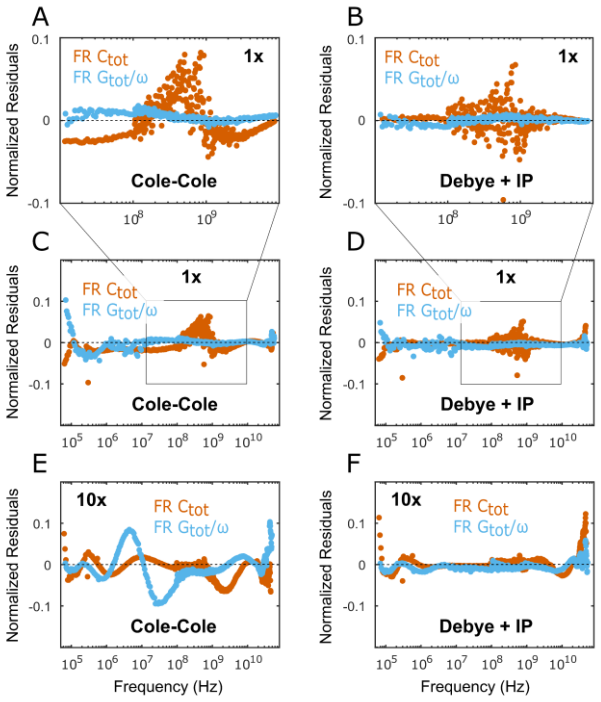

Fig. 4. Normalized fit residuals (FR) for C_{tot} and G_{tot}/ω for both 1× and 10× TAE-Mg^{2+} concentrations comparing the 'Cole-Cole' to 'Debye+IP' models. 'Debye+IP' model results in a better goodness of fit compared with the 'Cole-Cole' model over the entire frequency range for both the 1× and 10× concentrations.

IV. Conclusion

We measured the broadband microwave spectrum of TAE-Mg^{2+} buffer from 100 kHz to 67 GHz to quantify the effects of IP interactions. We developed an electrical model for this system that included the effect of ion pairing and compared this model to a model without ion pairing. After fitting both potential models ('Debye+IP' and 'Cole-Cole') to our calibrated microwave data, we found that the 'Debye+IP' model produced a significantly better fit over the entire measured frequency range. These quantitative measurements of ion pairing demonstrate the applicability of broadband microwave microfluidics for characterization of biological and chemical solutions containing dissolved ions. More broadly, we expect that quantitative broadband measurements of ion-pairing will inform more sensitive narrowband measurements, offering both cost-effective and real-time assessment of ion-pairing effects in biological systems.

References

[1] K. Grenier *et al.*, "Recent Advances in Microwave-Based Dielectric Spectroscopy at the Cellular Level for Cancer Investigations," *IEEE Trans. Microw. Theory Techn.*, vol. 61, no. 5, pp. 2023–2030, May 2013.

[2] J. C. Booth, N. D. Orloff, J. Mateu, M. Janezic, M. Rinehart, and J. A. Beall, "Quantitative Permittivity Measurements of Nanoliter Liquid Volumes in Microfluidic Channels to 40 GHz," *IEEE Trans. Instrum. Meas.*, vol. 59, no. 12, pp. 3279–3288, Dec. 2010.

[3] C. A. E. Little, N. D. Orloff, I. E. Hanemann, C. J. Long, V. M. Bright, and J. C. Booth, "Modeling electrical double-layer effects for microfluidic impedance spectroscopy from 100 kHz to 110 GHz," *Lab Chip*, vol. 17, no. 15, pp. 2674–2681, Jul. 2017.

[4] S. Liu *et al.*, "Hybrid Characterization of Nanolitre Dielectric Fluids in a Single Microfluidic Channel Up to 110 GHz," *IEEE Trans. Microw. Theory Techn.*, vol. 65, no. 12, pp. 5063–5073, Dec. 2017.

[5] X. Bao *et al.*, "A Planar One-Port Microwave Microfluidic Sensor for Microliter Liquids Characterization," *IEEE J. Electromagn. RF Microwaves Med. Biol.*, vol. 2, no. 1, pp. 10–17, Mar. 2018.

[6] R. Buchner, Stephen G. Capewell, A. Glenn Hefter, and P. M. May, "Ion-Pair and Solvent Relaxation Processes in Aqueous Na2SO4 Solutions," *J. Phys. Chem. B*, vol. 103, no. 7, pp. 1185–1192, Jan. 1999.

[7] S. I. Mamatkulov, K. F. Rinne, R. Buchner, R. R. Netz, and D. J. Bonthuis, "Water-separated ion pairs cause the slow dielectric mode of magnesium sulfate solutions," *J. Chem. Phys.*, vol. 148, no. 22, p. 222812, Jun. 2018.

[8] Y. Marcus and G. Hefter, "Ion pairing," *Chem. Rev.*, vol. 106, no. 11, pp. 4585–4621, Oct. 2006.

[9] R. Buchner, T. Chen, and G. Hefter, "Complexity in 'Simple' Electrolyte Solutions: Ion Pairing in MgSO 4 (aq)." *J. Phys. Chem. B*, vol. 108, no. 7, p. 2365-2375, Jan. 2004.

[10] X. Ma *et al.*, "A Multistate Single-Connection Calibration for Microwave Microfluidics," *IEEE Trans. Microw. Theory Techn.*, vol. 66, no. 2, pp. 1099–1107, Feb. 2018.

[11] N. C. Stellwagen, C. Gelfi, and P. G. Righetti, "The free solution mobility of DNA," *Biopolymers*, vol. 42, no. 6, pp. 687–703, Nov. 1997.

[12] A. C. Stelson, C. E. Little, N. D. Orloff, C. J. Long, and J. C. Booth, "Measuring Ion-Pairing in Buffer Solutions with Microwave Microfluidics," in 2018 IEEE International Microwave Biomedical Conference (IMBioC), 2018, pp. 127–129.

[13] D. F. Williams, C. M. Wang, and U. Arz, "An optimal multiline TRL calibration algorithm," *IEEE MTT-S International Microwave Symposium Digest*, vol. 3, pp. 1819–1822, Jun. 2003.

[14] D. C. DeGroot, J. A. Jargon, and R. B. Marks, "Multiline TRL revealed," in 60th ARFTG Conference Digest, 2002., pp. 131–155.

[15] N. D. Orloff *et al.*, "A Compact Variable-Temperature Broadband Series-Resistor Calibration," *IEEE Trans. Microw. Theory Techn.*, vol. 59, no. 1, pp. 188–195, Jan. 2011.

[16] N. D. Orloff et al., "How to extract distributed circuit parameters from the scattering parameters of a transmission line," in 90th ARFTG Microwave Measurement Symposium, 2017, pp. 1–5.

2469-7249 (c) 2018 IEEE. Personal use is permitted, but republication/redistribution requires IEEE permission. See http://www.ieee.org/publications_standards/publications/rights/index.html for more information.

This article has been accepted for publication in a future issue of this journal, but has not been fully edited. Content may change prior to final publication. Citation information: DOI 10.1109/JERM.2019.2896719, IEEE Journal of Electromagnetics, RF and Microwaves in Medicine and Biology

[17] W. Wachter, W. Kunz, and R. Buchner, "Is There an Anionic Hofmeister Effect on Water Dynamics? Dielectric Spectroscopy of Aqueous Solutions of NaBr, NaI, NaNO3, NaClO4, and NaSCN," *J. Phys. Chem.*, no. 109, pp. 8675–8683, Sep. 2005.
[18] R. Buchner, J. Barthel, and J. Stauber, "The dielectric relaxation of water between 0 °C and 35 °C," *Chem. Phys. Lett.*, vol. 306, no. 1–2, pp. 57–63, Jun. 1999.
[19] J. Ross Macdonald, "Note on the parameterization of the constant-phase admittance element," *Solid State Ionics*, vol. 13, no. 2, pp. 147–149, May 1984.
[20] X. Sun, S. Hyeon Ko, C. Zhang, A. E. Ribbe, and C. Mao, "Surface-Mediated DNA Self-Assembly," *J. Am. Chem. Soc.*, vol. 131, no. 37, pp. 13248–13249, Sep. 2009.
[21] M. Z. Bazant, K. Thornton, and A. Ajdari, "Diffuse-charge dynamics in electrochemical systems." *Phys. Rev. E*, vol. 70, no. 2, pp. 21506, Aug. 2004.

Charles A. E. Little (Cully) received his B.S. in Physics from Appalachian State University in Boone, NC, USA (2008). Afterwards, he worked as a research assistant in the Neutrino Group within the Physics Department at Duke University in Durham, NC, USA. He received his M.S. in Mechanical Engineering in 2013 and Ph.D. in Mechanical Engineering in 2017 from the University of Colorado in Boulder, CO, USA. His graduate research concerned developing techniques for microfluidic-based broadband measurements of fluid permittivity and permeability. He is currently continuing his work in the RF Electronics group at the National Institute of Standards and Technology in Boulder, CO, USA.

Angela C. Stelson received her B.S. in Physics, Mathematics, and Political Science from the University of Oregon in Eugene, OR, USA (2012), and her Ph.D. in Materials Science and Engineering from Cornell University in Ithaca, NY, USA (2017). Her graduate work focused on the electric-field directed assembly of colloids for photonic crystals. She joined the National Institute of Standards and Technology as a National Research Council Fellow in 2017. Currently, she works in the RF Electronics group developing new microwave microfluidics measurement techniques for medical diagnostics, pharmaceutical and materials science applications.

Nathan D. Orloff received his B.S. (Hons.) and Ph.D. degrees in physics from the University of Maryland at College Park, College Park, MD, USA, (2004 and 2010 respectively). His doctoral thesis involved the study and extraction of microwave properties of Ruddlesden-Popper ferroelectrics. In 2011, he joined the Department of Bioengineering, Stanford University, Stanford, CA, USA, as a Dean's Post-Doctoral Fellow with Prof. I. Riedel-Kruse. In 2013, he joined the Materials Measurement Laboratory, National Institute of Standards and Technology (NIST), Gaithersburg, MD, USA, as a Rice University Post-Doctoral Fellow with Prof. M. Pasquali. In 2014, he joined the newly formed Communications Technology Laboratory, NIST, to lead the Microwave Materials Project.
Dr. Orloff was a recipient of the 2004 Martin Monroe Undergraduate Research Award, the 2006 CMPS Award for Excellence as a Teaching Assistant, the 2010 Michael J. Pelczar Award for Excellence in Graduate Study, and the 2015 Communications Technology Laboratory Distinguished Associate Award.

Christian J. Long received the B.S. and Ph.D. degrees in physics from the University of Maryland at College Park, College Park, MD, USA, in 2004 and 2011, respectively. His doctoral research focused on the development of both microwave near-field scanning probe microscopy techniques and new methods to analyze data from combinatorial materials experiments.
From 2012 to 2015 Dr. Long was a postdoctoral researcher with the National Institute of Standards and Technology (NIST), Gaithersburg, USA, where he focused on techniques for characterizing nanoscale materials. In 2016, he joined the staff at NIST, Boulder, USA, where he currently leads a project on development of on-chip standards for microwave and mm-wave calibration.

James C. Booth received his B.A. degree in physics from the University of Virginia, Charlottesville, VA, USA (1989). He received his Ph.D. degree in physics from the University of Maryland, College Park, MA, USA (1996), where the subject of his dissertation was "Novel measurements of the frequency dependent microwave surface impedance of cuprate thin film superconductors."
He has been a physicist at the National Institute of Standards and Technology (NIST) in Boulder, CO, USA, since 1996, originally as an NRC postdoctoral research associate (1996-1998) and currently as Leader of the RF Electronics Group within the Communications Technology Laboratory. His research at NIST is focused on quantifying the microwave properties of new electronic materials and devices, including piezoelectric, ferrite, magneto-electric and superconducting materials, as well as linear and nonlinear measurements and modeling of analog components such as transmission lines and filters.
Dr. Booth was the recipient of a Department of Commerce Bronze Medal in 2015 for the development and application of measurements to determine electrical properties of thin-film materials over a range of frequencies from a few hertz to the terahertz regime.

2469-7249 (c) 2018 IEEE. Personal use is permitted, but republication/redistribution requires IEEE permission. See http://www.ieee.org/publications_standards/publications/rights/index.html for more information.